The Importance of Human Motion for Simulation Testing of GNSS

Kimon Voutsis, Paul D Groves, *University College London, United Kingdom*
Mark Holbrow, Colin Ford, *Spirent Communications plc, United Kingdom*

BIOGRAPHY

Kimon Voutsis is a PhD student of the Space Geodesy and Navigation Laboratory (SGNL) at University College London (UCL). He is interested in positioning sensors and navigation systems, human biomechanics and routing models. The aim of his current research is the development of a pedestrian motion model intended for testing the performance of positioning sensors in a simulation environment. He holds a first-class Bachelor (Hons) in Geography from Harokopio University of Athens, Greece and an MSc in Geographic Information Science from UCL. He has worked for three years in technical analysis and developing GIS software solutions for the transport industry. (k.voutsis.11@ucl.ac.uk)

Dr Paul Groves is a Lecturer (academic faculty member) at UCL, where he leads a program of research into robust positioning and navigation within SGNL. He joined in 2009, after 12 years of navigation systems research at DERA and QinetiQ. He is interested in all aspects of navigation and positioning, including multi-sensor integrated navigation, improving GNSS performance under challenging reception conditions, and novel positioning techniques. He is an author of more than 60 technical publications, including the book Principles of GNSS, Inertial and Multi-Sensor Integrated Navigation Systems, now in its second edition. He is a Fellow of the Royal Institute of Navigation and holds a bachelor's degree and doctorate in physics from the University of Oxford.

Mark Holbrow has worked with Spirent Communications (formerly STC, Nortel and Global Simulation Systems) for 20 years. Key responsibilities throughout that period have been in the design and development, and now the management and direction, of Spirent's extensive range of GNSS RF Simulation and Inertial Test Systems. He holds an MEng in Communications, Information and Electronic Engineering from University Of Plymouth, Devon, England.

Colin Ford is Staff Software Engineer at Spirent Communications plc.

ABSTRACT

Human motion is generally considered benign to the performance of global navigation satellite system (GNSS) and other positioning sensors. This study proves that this is not the case, even for typical human behaviour involving GNSS user equipment, e.g. in smartphones. Using recorded human motion, it is shown that phase-lock loops (PLLs) in GNSS receivers are sensitive to jerk dynamics induced by user motion, resulting in carrier cycle slips.

To test the effects of human dynamics on GNSS carrier tracking, real human motion profiles were captured. These profiles comprised typical types of movements using a mobile phone, e.g. holding, answering and texting, different types of activities, e.g. walking or jogging, as well as different phone locations on the human body, e.g. in a hand, pocket, backpack and on an arm band. The data were captured outdoors using an Xsens MTi-G MEMS (Micro-Electronic Mechanical Systems) Inertial Measurement Unit (IMU) aided by a Global Positioning System (GPS) receiver with a 100Hz output rate. Then the captured motion (MoCap) was processed and input into a simulated PLL in Matlab with different tracking loop bandwidths (B_{L_CA}) and carrier power-to-noise density ratios (C/N_0).

The results show that pedestrian gestures and type of activity, e.g. walking or jogging, affect the performance of the simulated PLL more adversely than the location of the phone on the human body. Also, to track pedestrian motion encompassing these gestures, activities and receiver locations, a minimum of 15Hz tracking bandwidth is required. Consequently, receiver manufacturers should exercise caution before reducing tracking bandwidths to compensate for the reduction in C/N_0 resulting from GNSS antenna design, human body masking and the effects of buildings, trees and other environmental features.

This paper also proposes and describes a pedestrian motion model (PMM) that simulates the GNSS antenna trajectory in 3D, when it is held by or attached to a pedestrian. The PMM will be validated using real MoCap scenarios and will enable Spirent to increase their product offering in the area of simulation-based testing of positioning sensors for pedestrian applications by generating human motion profiles which affect realistically the performance of GNSS user equipment.

1. INTRODUCTION

Providing a truth reference model is key to testing positioning devices' performance both in field trials and simulation environments, especially for pedestrian applications where the great variability of human motion induces additional challenges. Human activities and the context where they take place, involve many different types of motion, e.g. walking, running, side-stepping, ascending/descending stairs etc., and encompass particular motion quantities, such as position, attitude, linear or angular velocity, acceleration and jerk (acceleration rate of change). These specific motion characteristics in turn may, or may not, have an impact on GNSS sensors' performance, e.g. those inside smartphones, by inducing phase cycle-slips and false frequency locks in the carrier phase and frequency tracking functions of the GNSS receiver [1][2][3]. Therefore, to design a truth reference model for testing positioning devices for pedestrians, it is essential to study the motion characteristics of human motion within a given context and how it affects the performance of GNSS receivers. This study will support the development of an application where a user can drive a PMM to recreate realistically the effects of human motion on GNSS receivers.

Human motion is generally considered benign to the performance of GNSS and other positioning sensors. This study proves that this is not the case, even for 'day-to-day' pedestrian behaviour involving GNSS user equipment. Using recorded human motion, it is shown that phase-lock loops (PLLs) in GNSS receivers are sensitive to jerk dynamics induced by human motion, resulting in carrier cycle slips. The receiver performance for pedestrian navigation therefore depends on where the antenna is placed and the type of activity, e.g. walking or jogging. Human motion is also subject to great variability depending on individual characteristics, e.g. gender, health status [2]. Therefore, appropriate modelling of human motion is critical for testing its effects on GNSS receivers. This study proposes a method of modelling human motion, using a human biomechanical model (HBM), also called "humanoid", "anthropoid", or "human skeleton" by other authors, which will be driven by a pedestrian routing model (PRM) in order to simulate the 3D trajectory of a GNSS antenna, held by or attached to a pedestrian. The output of the proposed PMM will be compared in the future with human MoCap data to ensure that both have the same effect on GNSS carrier tracking loops.

This paper is organised as follows. Section 2 introduces briefly the state of the art in the areas of human motion capture and modelling and how human motion affects GNSS carrier-tracking. Section 3 presents the proposed method for modelling human motion and how to simulate its effects on GNSS carrier tracking loops. Section 4 details the results of the human MoCap experiments conducted to study carrier tracking performance in the presence of this motion. Finally, Section 5 summarises the conclusions of the present study and Section 6 discusses the future work which will be carried out to complete the project.

2. BACKGROUND

This Section outlines the underlying thematic areas of this study, namely human motion capture and modelling, as well as carrier tracking loops in GNSS receivers. These topics encompass the concepts and tools that will help to address the problem statement of this paper, i.e. how human motion can affect the performance of GNSS receivers in terms of inducing artificial cycle slips in carrier phase-tracking loops.

2.1 Human motion: capture and modelling

Human motion can be captured by a range of different sensors or their combinations. For clinical applications, optoelectronic systems using active or passive markers are standard [4], or IMUs, which typically encompass a triad of accelerometers and gyros. IMUs are self-sufficient devices in terms of providing a position and attitude solution without the need of any other external sources of information, e.g. radio signals. IMUs' range of applications spans from everyday use, e.g. inside car navigation systems or smartphones, to special military applications, e.g. ballistic missiles. In [5], the authors assess how suitable inertial sensors are for the study and analysis of human motion, concluding that they have the potential to be employed in clinical applications involving walking. Due to the wide range of applications that employ IMUs (as part of Inertial Navigation Systems) with different performance requirements, IMU performance grades may be categorised into consumer or automotive, tactical, intermediate, aviation, and marine grades, as detailed in [1]. According to this categorisation, the Xsens MTi-G IMU used in this study, is on the boundary between consumer and tactical grades, although there is no uniform definition of these categories among authors.

An essential part of using IMU sensors for human MoCap is the static bias calibration of the constituent inertial sensors. The Xsens MTi-G IMU/GPS allows calibration of the static bias of the accelerometers, by performing manoeuvres prior starting the MoCap. A typical pre-calibrated MEMS IMU, such as the Xsens MTi-G, is subjected to 0.02 m/s^2 accelerometer static bias (1σ) and 1 deg/s gyro static bias (1σ) [6].

Another important aspect of human MoCap, using an IMU/GNSS device, is the GNSS antenna location on the human body. Ideally, the selected sensor locations, should allow for good GNSS signal reception during MoCap experiments. In addition, due to the fact that human body motion has many DOF, the sensor location must be carefully selected as human motion may block GNSS signals or induce relative motion dynamics between the GNSS antenna and the IMU.
The study of human body motion will support the development of a PMM in this project. Human

biomechanics involve the study of mechanical properties of human body elements, e.g. muscles and bones. In this project, the focus is on human locomotion, i.e. the movement of a human being between two locations, and human gait analysis, which studies the mechanical properties of the human body during gait (e.g. walking, running etc.), as well as human gestures and different GNSS receiver locations on the human body [7]. Any movement of a human segment (or the body as a whole) encompasses up to 6 degrees of freedom (DOF), three for translational (or linear) motion and three for rotational (or angular) motion. These translational and rotational components are referenced along and about, respectively, a system of three orthogonal axes which intersect at the human centre of mass (CoM) when a human being is standing, as illustrated in Figure 1. This system of axes comprises X – anteroposterior axis (positive is forward), Y – mediolateral axis (positive is right) and Z – longitudinal axis (positive is down), also shown in Figure 1.

The human body movement can be modelled using biomechanical models, examples can be found in [8][9]. These models contain a simplified version of human body segments, e.g. modelled as cylinders or spheres, and motion constraints between these segments, which represent the mechanical properties and DOF of human joints. Using a human biomechanical model (HBM), it is possible to simulate particular type of activity, e.g. walking, jogging, and/or gestures. Human gesture examples include moving arms back and forth, answering a phone, turning the head, kicking with a foot etc.

Human gait comprises a repeatable series of similar steps, with linear displacement of the CoM along the three axes of the pedestrian body frame (illustrated in Figure 2), reflecting the variable change of support of the upper part of the body by the legs. The analysis of particular human body segments' movement during gait, e.g. trunk movement, hand gestures etc. can be carried out w.r.t. the human gait cycle. A human gait cycle involves distinct events (as shown in Figure 2), such as heel contact, heel rise, toe off, feet adjacent, tibia vertical and (again) heel contact of the reference leg, which initiates the next gait cycle.

The human CoM is equivalent to the centre of gravity (CoG) and represents the point around which all particles of the human body are evenly distributed. The most interesting property of CoM movement, at least within the scope of this project, is that it follows a sinusoidal motion both in the mediolateral axis (projected on the frontal plane) and the vertical/longitudinal axis (projected on the sagittal plane) during the human gait cycle. This hypothesis is accepted by many studies in human biomechanics [10][11][12][13][14][15][16]. More specifically, the CoM describes two vertical and one mediolateral oscillations per gait cycle independently of the walking or running speed [17]. In practice, human gait is far more complex than simple mechanical models can represent, since joints and segments present additional translational and rotational DOFs during gait, e.g. the relative linear motion between pelvis (encompassing the CoM) and trunk [13].

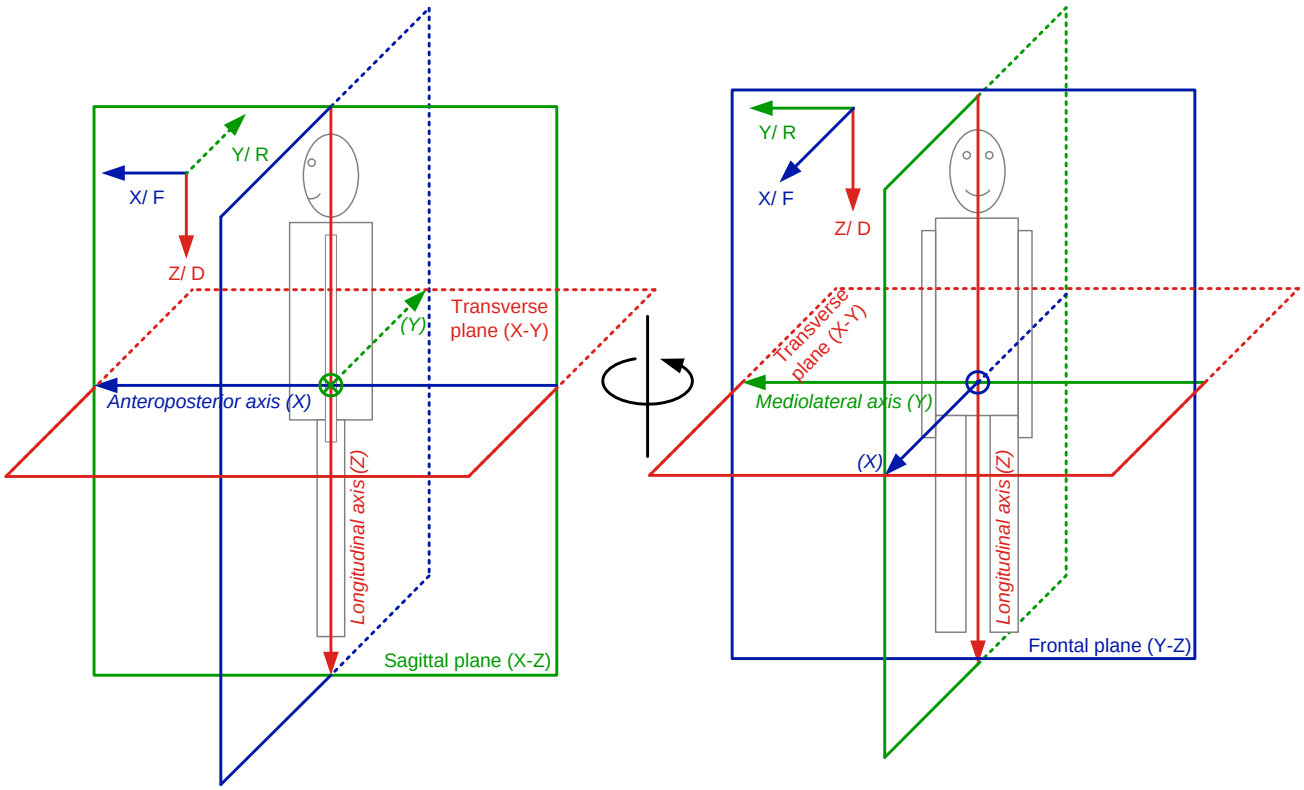

Figure 1. Pedestrian body frame axes and planes intersecting at the CoM

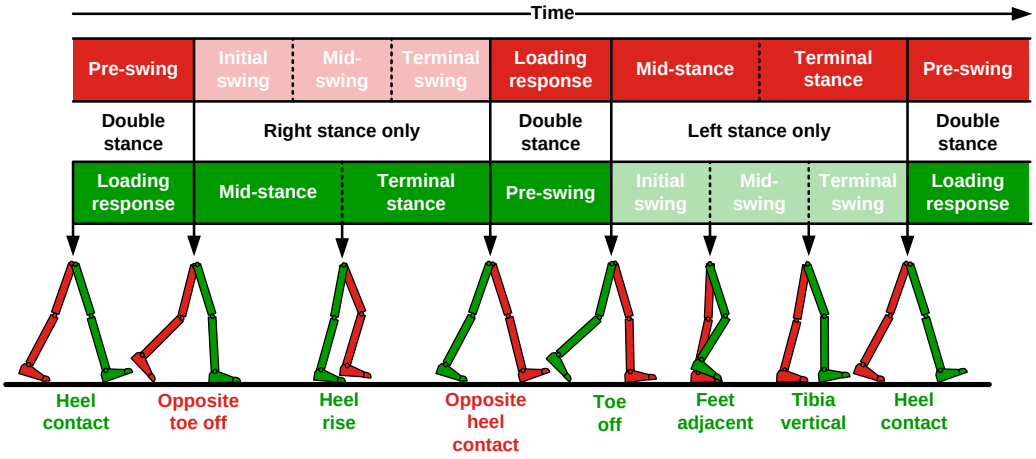

Figure 2. Events and phases during one human gait cycle (after [10])

Finally, an essential element of human motion modelling for this project, is to study how a pedestrian navigates in the environment (2D or 3D space). Pedestrian navigation encompasses two basic actions, routing (also called "way-finding", "path-finding" or "route-finding" by other authors) and positioning [1]. Positioning involves the determination of user position at a given time with respect to (w.r.t.) a known frame of reference, while pedestrian routing encompasses a geographic goal which the pedestrian aims to reach by moving in 3D space. In this study, a pedestrian routing model (PRM) will drive an HBM along a route between two pre-defined geographic points. A standard method of finding the optimal (shortest) path between two nodes in a graph is Dijkstra's algorithm [18], which can also be adapted to grid space representations. Essentially, Dijkstra's algorithm starts from a certain node and expands gradually the search around that node, until the finish node is reached, provided that there is at least one path connecting the start and finish nodes. The review of versions of Dijkstra's algorithm which are optimised for processing speed purposes, are beyond the scope of this project.

2.2 Carrier tracking loops in GNSS receivers

Carrier tracking of GNSS signals aims at estimating the Doppler shift of the carrier frequency and, in some receivers, carrier phase error, in order to achieve more precise alignment between the pseudo-random noise (PRN) code, which is modulated in the incoming GNSS satellite signal, and the receiver-generated (replica) PRN codes. This process takes place in the GNSS receiver's signal processor over the coherent time interval [1] [19][20]. Carrier tracking is normally implemented via tracking loops, although other methods may encompass Kalman Filter [21][22][23][24][25][26], or Fast Fourier Transform algorithm to track carrier phase and frequency in the frequency domain [27].

This study will examine the effect of human motion on the performance of a typical phase lock loop (PLL), noting that carrier range (units in m) is the equivalent of phase (units in rad) in the range domain, which will be used for the present analysis. Another type of carrier tracking loops is a frequency lock loop (FLL), which tracks carrier range rate (the equivalent of frequency in the range domain). PLLs are less robust than FLLs in terms of motion dynamics along the line-of-sight (LOS) between the user equipment and the GNSS satellite, as well as C/N_0 [1][19][20]. However, PLLs allow more precise alignment of the incoming and replica PRN codes than FLLs, for precision estimation of the code phase and the time of the GNSS signal arrival. Due to their different design and performance characteristics, some GNSS receivers combine a PLL aided by a FLL in order to maintain lock of the signal [27][28].

First-order PLLs can track carrier range error only (thus not applicable to GNSS signal tracking), second-order PLLs can track carrier range and range rate errors, while third-order PLLs can track carrier range, range rate and range acceleration errors. Similarly, first-order FLLs can track carrier range rate error and second-order FLLs can track carrier range rate and range acceleration errors. The purpose of a PLL is to minimise the carrier range error, in order to maintain alignment between the incoming and replica GNSS signals over the coherent correlation time interval [1].

An example of a third-order PLL is illustrated in Figure 3. The accumulated correlator outputs (Is and Qs) are sampled and accumulated to be input into a carrier range discriminator function that detects a carrier range error, which is then normalised depending on the standard deviation of the discriminator function, the correlator accumulation time interval τ_α and the C/N_0 (obtained by the signal processor) [1][3][20]. The accumulation interval of the Is and Qs inside the PLL defines the PLL bandwidth, i.e. the output rate to the numerically-controlled oscillator (NCO). The carrier range error is smoothed and used, inside the PLL filter, to update the current carrier range, range rate and range acceleration estimates, noting that the range acceleration remains unchanged. Then, these current range estimates are used to predict the range, range rate and range acceleration which will feed the PLL filter in the next loop iteration, i.e. after a τ_α time interval, in order to re-update the current (at that epoch) carrier range, range rate

and range acceleration estimates. It is worth noting that during these loop iterations the range acceleration estimate remains unchanged in a third-order PLL. Also, the range predictions are sent to the numerically controlled oscillator (NCO) to control the generation of the receiver-generated replica carrier signals, in order to keep them aligned with the incoming GNSS signal in the signal processor's correlators.

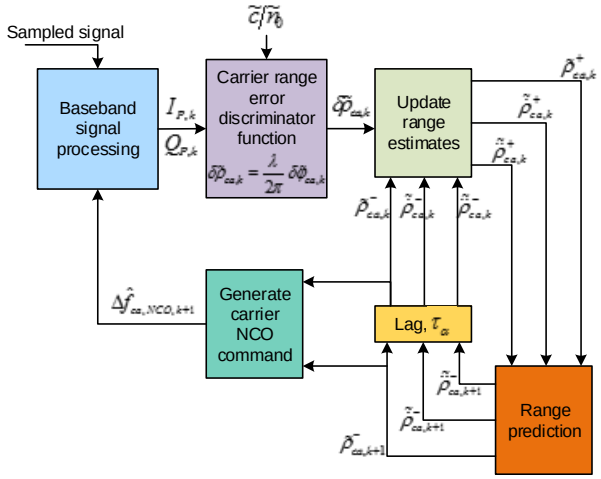

Figure 3. An example of a phase-lock loop (after [1]).

A PLL allows more precise tracking of the carrier, as it estimates the carrier phase, but it is less robust due to the sensitivity to noise and dynamic stress [1][20]. The error sources of PLLs are as follows [29]:

- *Vibration-induced* phase noise to the NCO; this can be internal noise cause by frequency standard instabilities of the NCO itself. These effects are also explained in [19].
- *Thermal* and *RF* (Radio-Frequency) noise, which is always present in electronic circuits and is independent of the PLL order. RF noise includes the other GNSS signals on the same frequency and other interference sources. A more detailed study of the effects of thermal noise and oscillator phase noise to the performance of PLLs is presented in [30].
- *Dynamic stress* error due to the relative motion between the satellite and the GNSS receiver which tracks the signal of that satellite. This depends on the order of the PLL, with first, second and third order PLLs sensitive to velocity acceleration and jerk stress respectively.

Vibration-induced noise, thermal and RF noise and multipath effects, which also have an impact on carrier tracking loops' performance [19], are out of the scope of this study. Typically, PLL carrier phase errors are in the order of 1.2mm (1σ) under good C/N_0 [3], e.g. for C/N_0 higher than 40dB-Hz.

A perfect alignment of the incoming and replica GNSS signals, results in a complete removal of the PRN code from the GNSS signal (code wipe-off), but the incoming GNSS signal still contains the modulated navigation message (at a rate of 50bit/s), using a binary phase shift keying (BPSK) modulation. BPSK modulates the navigation bits transition in the carrier by altering the phase of the signal by π rad.

A Costas discriminator has a carrier tracking error input range of ($-\lambda_{ca}/4$, $\lambda_{ca}/4$) m, where λ_{ca} the GNSS carrier wavelength, so it is not sensitive to navigation bit transitions which change the phase of the incoming signals by $\lambda_{ca}/2$ m. Other types of discriminators are described in [1], noting that the choice of a particular discriminator design depends on the hardware complexity of the GNSS receiver, and the performance requirements of the user application. For human motion, it is considered that an arctan discriminator is more robust, as the gain (slope of input-output curve) is linear over the carrier tracking error input range, as illustrated in Figure 4. If the carrier range tracking error, $\delta\rho_{ca}$, exceeds the pull-in range of a Costas discriminator, this will cause the discriminator to observe a range error which is a multiple of $\lambda_{ca}/2$ m, for a Costas two-quadrant arctan discriminator (shown in Figure 4), or a multiple of λ_{ca} m, for a four-quadrant arctan PLL discriminator [1][20]. This error is called a cycle-slip and it affects the navigation message demodulation and carrier-based ranging [1], which is critical for precise positioning, as it may span from one cycle-slip to millions of cycle slips in extreme cases. Carrier range tracking errors may exceed the pull-in range of the discriminator, due to receiver motion dynamics or low C/N_0, where the receiver may lose lock of the signal and until the lock is re-obtained, multiple cycle-slips may have occurred due to a large pseudo-range change. Cycle slips may also occur due to reference oscillator errors, e.g. due to temperature variations, crystal physical characteristics and aging, sensitivity to gravity force causing frequency variations and vibration sensitivity causing phase noise in the oscillator and random high-frequency phase noise [19], but these effects are out of the scope of this project.

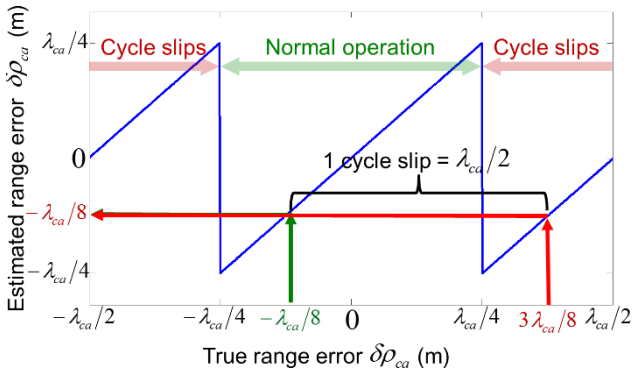

Figure 4. Example of a cycle slip in a Costas arctan (two-quadrant) discriminator.

A phase lock loop (PLL) acts as a low pass filter due to its low bandwidth; for applications that do not require tracking of high dynamics, e.g. for static receivers a low bandwidth is common, while for high dynamics applications up to 20Hz may be used [31]. For a PLL with a bandwidth B_{L_CA} = 20Hz (i.e. a fast response to motion

dynamics), the maximum jerk tolerance over the coherent time interval (typically 0.02s) will be about ±657m/s^3, for B_{L_CA} = 10Hz about ±82m/s^3, and for a B_{L_CA} = 5Hz (a slow response to dynamics) about ±10m/s^3, noting that larger (absolute) jerk dynamics may occur over smaller time intervals (less than 0.02s) without causing cycle slips [1]. Typically, carrier phase tracking can be maintained when C/N_0 is above 24dB-Hz depending on PLL bandwidth and motion dynamics [19]. The following Section explains how this paper will assess the impact of pedestrian induced motion dynamics on GNSS carrier phase-tracking, by capturing and modelling human motion, and also, by simulating a third-order PLL in Matlab.

3. METHOD

This Section details the process of capturing human motion data in the field, and continues by proposing and describing a custom pedestrian motion model which aims to recreate realistically the human motion profiles in a simulation environment. This Section concludes by presenting how the captured motion profiles were input to the third-order PLL, which was simulated in Matlab.

3.1 Human Motion Capture

To test the effects of human dynamics on GNSS carrier tracking, real human motion profiles were captured. These profiles comprised both scenarios where the person is using a mobile phone, i.e. walk holding, answering and/or texting, and scenarios where the phone is carried at different locations on the human body, e.g. in a pocket, in a bag, or on an arm band, as detailed in Table 1:

MoCap scenario name	Description
L_H_W30m_S	Walk 30m holding the phone, then stop
L_P_W30m_S	Walk 30m, phone in the pocket, then stop
L_B_W30m_S	Walk 30m, phone in a backpack, then stop
L_A_W30m_S	Walk 30m, phone in an arm-band, then stop
L_H_W15m_A_W15mS_D	Hold the phone, walk 15m, answer the phone then stop and put the phone down
L_P_W15m_A_W15mS_D	Phone in the pocket, walk 15m, answer the phone then stop and put the phone down
L_H_W15m_T_W15mS_D	Hold the phone, walk 15m, send a text, stop and put the phone down
L_P_W15m_T_W15mS_Dh	Phone in the pocket, walk 15m, send a text, stop and put the phone down
L_H_J30mS	Jog 30m holding the phone, then stop
L_P_J30mS	Jog 30m, phone in the pocket, then stop

Table 1. Descriptions of MoCap scenarios

The MoCap data were captured outdoors using an Xsens MTi-G IMU/GPS device with a 100Hz output rate. The user walked horizontally in a straight line for 30m and then back, holding the phone. The final motion profile was generated from the integrated Xsens IMU/GPS position solution. However, this exhibits discontinuities due to the GPS-derived corrections to the inertial solution following each Kalman Filter measurement update. As well as producing an unrealistic motion profile, it also causes additional cycle slips in the GNSS tracking simulation. Therefore, a custom filter has been developed to smooth out the transient effects of these GPS updates, without smoothing the underlying motion. Consequently, the GNSS tracking simulations should only exhibit cycle slips due to the actual motion, not due to artefacts of the motion capture process. Figure 6 shows this effect in an extract of recorded motion, where the user is holding the GNSS antenna by the right ear (i.e. answering the phone) while walking 6 steps. For this reason, in this paper the inertial-only solution was used to drive the simulated PLL, as it does not contain any artificial GPS transients, which can disrupt the performance of carrier phase tracking by introducing artificial cycle slips.

Figure 5 illustrates the workflow of the MoCap experiments. The equipment is set-up and then recording starts (video camera and MoCap from the IMU/GPS device user interface – MT Manager). The IMU/GPS device is calibrated for the accelerometer and gyro biases, ensuring that it is subject to significant horizontal acceleration prior to the actual motion capture phase. Then the user goes to the initial position and performs event-based synchronisation (EBS) between the IMU/GPS device and the video camera; this usually involves moving the IMU/GPS device up and down for five times. The user performs the motion scenario in question and, when finished, performs EBS again. The EBS process is particularly important in order to identify the start and finish time instants of the actual motion when post-processing the captured data.

A proprietary Kalman Filter is used internally in the Xsens MTi-G in order to correct the inertial position, velocity and attitude solutions using GPS updates. The inertial and GNSS navigation solutions (position and velocity) are fed into the integration algorithm which calculates the error states, e.g. accelerometers and gyro biases, attitude (pitch, roll and yaw/heading) biases, and not the original quantities themselves (e.g. specific force or angular rate). It is, therefore, a complementary filter. These errors are then used in a correction stage to update the inertial navigation solution and provide the integrated navigation solution (position, velocity and attitude), noting that the Xsens Kalman Filter is proprietary so the end user cannot amend the actual implementation.

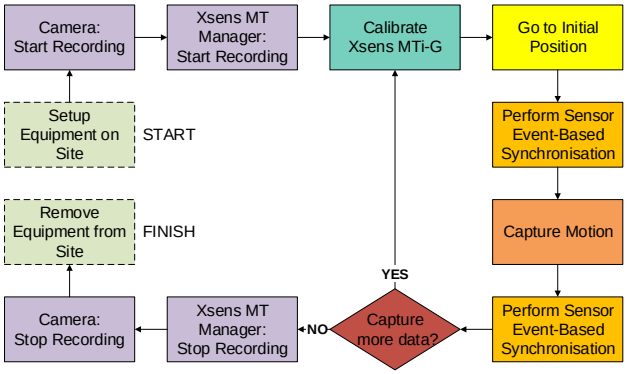

Figure 5. Motion capture workflow

The Xsens Kalman Filter selected to process the human MoCap data in this project does not involve magnetometers. As a result, the Kalman Filter can only observe the heading error when GNSS signals are available and the IMU is subject to significant horizontal acceleration that will create additional linear velocity and quadratic position errors to be observed by the Kalman Filter (see Figure 10), separately from velocity and positions errors (linear and quadratic, respectively) caused by tilt (pitch and roll) errors and accelerometer biases. Once the heading error has been observed and assuming that the tilt errors have also been observed, the Kalman Filter stabilises and the attitude solution can be corrected effectively. However, if the IMU stops experiencing horizontal acceleration, the Kalman Filter heading error observability will degrade. This implies that for human MoCap scenarios, continuous motion of the sensor is preferable. Also, it is possible to store the current Kalman Filter state (inertial sensor biases) and re-use it in the future for similar MoCap scenarios. In this way, the Kalman Filter does not have to settle again when post-processing the new MoCap data [6].

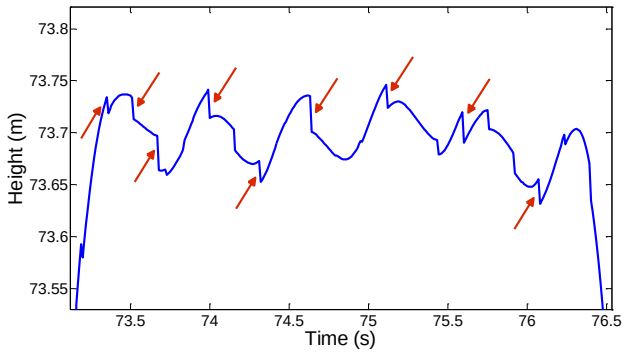

Figure 6. Example of GPS transients in Kalman Filter integrated height solution

3.2 Pedestrian Motion Model (PMM)

In the MoCap experiments of this project, the following candidate sensor locations on the human body will be considered: head, shoulder, upper arm, forearm, wrist, hand (held or attached) and center of thorax. These were selected based on the likely locations of GNSS antenna on the human body, noting that not all of these candidate locations allow for human gestures. Other types of gesture that may occur with the sensor located elsewhere, e.g. nodding the head when the sensor is placed on the top of the head, are outside the scope of this project.

Figure 7. The Xsens MTi-G IMU/GPS device with a GPS antenna

Figure 8. An example of using the Xsens MTi-G in a human MoCap experiment, with the antenna attached on the outside of the right hand and the IMU on the inside.

A particular antenna location on the human body may involve specific gestures, e.g. answering the phone when the sensor is placed on the hand, or nodding the head when the sensor is mounted on a helmet. Modelling of the GNSS antenna location on the human body and any potential human gestures involved for that particular location in question, is essential in order to reproduce realistically the 3D motion of a GNSS antenna and the effects on the performance of the GNSS receiver in the presence of this motion. In this project, a human gesture will be defined as the movement that a human body segment (on which the sensor is located) performs in addition to the normal human body movement during the gait cycle, as seen in Figure 1. Therefore, human gestures are additional movements that can be overlaid on the HBM, (see Table 2).

Simulating human motion requires a PRM to be combined with an HBM. The PRM implementation is based on Dijkstra's pathfinding algorithm [18]. It defines a path between two points in 3D space, which the HBM will be forced to follow. The HBM describes and controls the relative motion of different parts of the human body. It encompasses 17 constituent parts including pelvis,

abdomen, thorax, left/right upper arms, left/right lower arms, and left/right hands, see Figure 11. These parts can rotate w.r.t. their adjacent segments, forming a biomechanical (kinematic) chain which starts from the whole-body Center of Mass (CoM), inside the pelvis.

The output of the PRM will be processed, using a smoothing function, in order to produce a more realistic final route. Upon this smoothed route, more detailed human motion (i.e. the GNSS antenna trajectory encompassing human gestures) will be overlaid through the HBM. The integration of the PRM and HBM will produce the final 3D trajectory of the GNSS–equipped device between the two user-defined points of interest, which will represent the dynamics environment that the device is subjected to during this motion, i.e. the PMM.

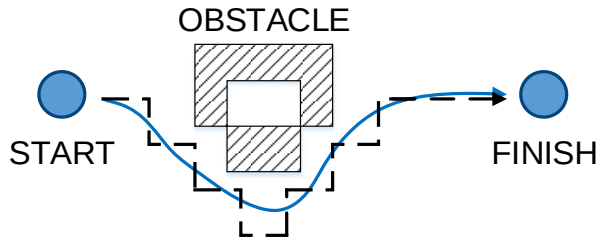

Figure 9. Example of a pedestrian routing model (PRM) via Dijkstra's algorithm (black line) and a smoothed version (blue line) of the calculated route

This approach, encompasses an analytical model describing human movement, e.g. three sinusoids to describe the forward/backward (X-axis), left/right (Y-axis) and up/down (Z-axis) displacements of the human CoM during human gait, as well as human gestures. Any human gestures which involve GNSS equipment will also have to be modelled using a system (or chain) of lever arms, as defined by the HBM in Figure 11, starting from the CoM point and finishing at the human segment where the GNSS equipment is held or attached. This will allow the modelling of a gesture, e.g. answering the phone, while the user performs a specific type of activity, e.g. walking. It must be noted, that an analytical model of human movement may be appropriately extended to encompass stochastic elements which might impact the performance of GNSS tracking loops, e.g. due to the muscles physiological tremor [32][33]. The advantage of this method is that it can represent pedestrians with different anatomical characteristics (e.g. gender, step length, cadence), noting that the validation of all possible combinations of the analytical model cannot be exhaustive.

Pedestrian Motion Model (PMM):
• Human Biomechanical Model (HBM)
○ GNSS antenna location
○ Type of activity
○ Gestures
• Pedestrian Routing Model (PRM)
○ Dijkstra's algorithm
○ Smoothing function

Table 2. Pedestrian motion model constituent elements

The fact that the HBM will have to follow a specific route (output from the PRM), renders a trials-based approach less flexible, as it would require collating a lot of basic MoCap elements to reproduce the final receiver trajectory, that could not be modified in the post-processing.

The HBM of Figure 11 consists of 17 segments marked with black lines, i.e. head/neck, trunk/thorax and pelvis, right/left shoulder, upper arm, forearm, hand, femur, shank and foot. Adjacent segments are connected by joints, marked by blue points, forming a biomechanical chain of segments, as illustrated in Figure 11. These joints have uniquely identifiable codes listed in Table 3. The total-body CoM position in 3D, can be calculated from [34], which explains how to calculate the total-body CoM coordinates w.r.t. a local frame of reference, using the mass of each segment relative to that of the total-body and the CoM of each segment, as obtained from a series of other anthropometric studies. The reference point "O" is the projection of the (HBM) CoM on the level floor.

Joint code	**Human body location**
JHN	Head/neck
JTP	Between trunk/pelvis
JRS	Right shoulder
JLS	Left shoulder
JRE	Right elbow
JLE	Left elbow
JRW	Right wrist
JLW	Left wrist
JRH	Right hip
JLH	Left hip
JRK	Right knee
JLK	Left knee
JRA	Right ankle
JLA	Left ankle
JRF	Right foot (heel)
JLF	Left foot (heel)

Table 3. List of joints and their locations on human body

The constituent segments of the proposed HBM, are normalised to 1,000 w.r.t. the height of the HBM to allow customisation for different individuals, based on anthropometric data tables [8]. Starting from the CoM point, whose 3D position can be described by the three-sinusoid model, the 3D translational motion of the segment joints can be calculated w.r.t. the CoM, knowing the rotations of the segments about the joints' centres and using the kinematic equations. The rotations of the joints involved in specific types of activities and/or gestures which are not already known from the human biomechanics literature, will be calculated from field experiments, involving simple methods, e.g. measure the angle between two adjacent body segments, or using more advanced gait analysis methods, as those reviewed in [4]. Sensor locations on the human body can be either on human joints (highlighted in blue in Figure 11) or intermediate positions. Figure 11 highlights the segments which will be used to model human gestures and sensor locations on the human body, by modelling their relative motion w.r.t. "O".

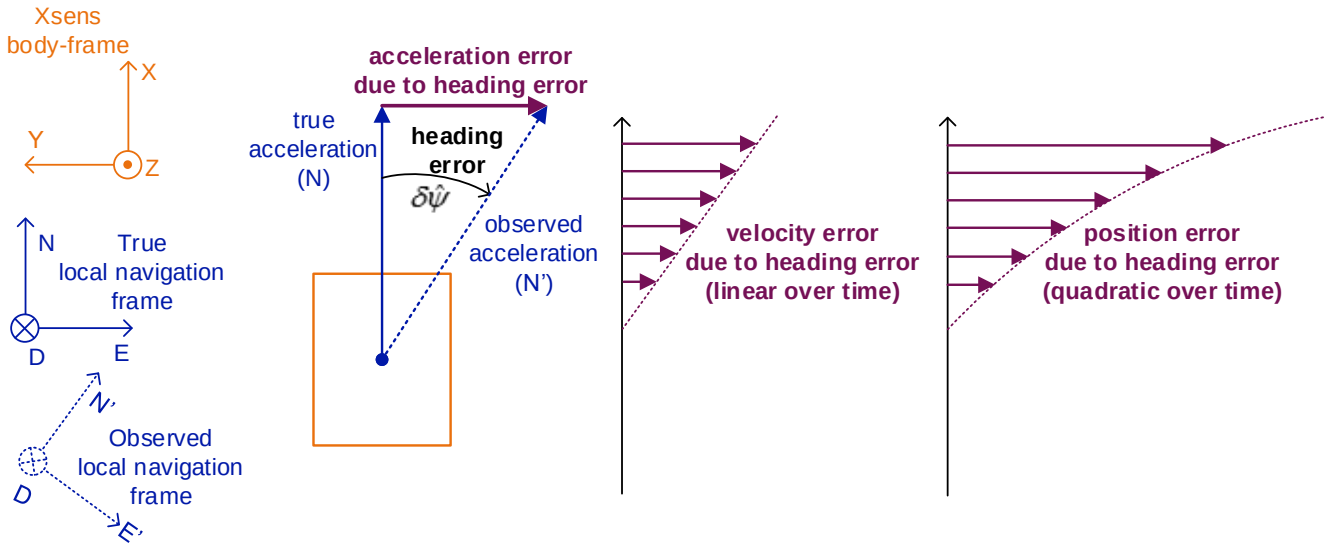

Figure 10. Example of how heading error in an IMU induces errors to observed velocity (linear) and position (quadratic).

Finally, the output of the PMM will be a synthetic trajectory which recreates realistically the motion of the sensor and thus the GNSS cycle-slip effects on a third-order PLL. The ultimate validation criterion for the developed PMM will be to recreate the same effects (cycle-slips) on GNSS tracking loops as the MoCap data.

3.3 GNSS Carrier-Tracking Loops Simulation

A third-order PLL, as described in Section 2.2 and illustrated Figure 3, was simulated in Matlab. The human MoCap profiles were converted from the range (position) and range rate (velocity) domains to the phase and frequency domains, respectively, and then used to generate I and Q signals (which are functions of phase and frequency error), using the equations from [1]. The generated I and Q signals were fed into the simulated PLL, and the output was used to control directly (without NCO modelling) the generation of I and Q signals in the next loop. This assumption was made because NCO noise dominates lower tracking bandwidths [19], which cannot respond fast enough in the presence of human motion.

A cycle-slip, explained in Section 2.2, is detected when the range error, i.e. the difference between the input range (truth reference as captured by Xsens MTi-G) and the predicted (observed) range by the simulated PLL exceeds the pull-in range of the phase (range) error discriminator. In the case of Costas phase (range) discriminator this condition is:

$$\left|\delta\rho_{ca,k}\right| > \frac{\lambda_{ca}}{4},$$

where $\delta\rho_{ca,k}$ is the range error (in m) and λ_{ca} is the carrier wavelength (in m).

4. RESULTS

The effect of human motion on GNSS carrier tracking is demonstrated using motion profiles recorded by an Xsens IMU/GPS device. This data is used to drive third-order carrier phase tracking loop in Matlab at a range of signal strengths and tracking bandwidths to determine the performance limits. The simulation tests involving human motion, assume three static satellites in the North, East and Down (NED) lines of sight, w.r.t. the user GNSS equipment for the duration of the movement and that the recorded motion is resolved along these lines of sight before it is input to the PLL simulation. Therefore, these results show the combined cycle-slip effect, in the presence of motion along any of the resolved NED lines of sight, on the simulated PLL. The simulations used a GPS L1 carrier wavelength of about 0.19m, and a correlator accumulation time interval of 0.01s. The simulation parameters encompass varying C/N_0, between 15dB-Hz and 45dB-Hz (31 cases), and PLL effective bandwidth (B_{L_CA}) between 5Hz and 20Hz (i.e. 16 cases). The effects of radio frequency and thermal noise (i.e. tracking noise), were modelled by white noise Monte Carlo sequences (random normal distribution sequences) using 400 different noise seeds, which were added to the generated in-phase and quadrature accumulated correlator outputs (I and Q signals). Totally, 198,400 (31 x 16 x 400) simulated cases were run for each input human motion profile.

In addition to motion profiles, a static (motionless) profile was input on the simulated PLL, i.e. a profile without motion dynamics (constant range and zero range rate) along any line of sight between the GNSS receiver and a satellite. This static profile was used as control data to study the response of the simulated PLL in the absence of motion dynamics, since the tracking noise, simulated by 400 different white noise seeds in Matlab, can also cause cycle slips on the simulated PLL. The result is illustrated in Figure 12. The black dotted line in Figure 12, represents

the minimum C/N_0 threshold required for the simulated PLL to operate without experiencing cycle-slips, at tracking bandwidths between 5Hz – 20Hz. The higher cycle-slip effects were observed when low C/N_0 and high PLL bandwidths were combined; this means that under these conditions, cycle-slips would occur anyway, irrespectively of the pedestrian manoeuvres involved in the input motion profile. In other words, any potential cycle slips occurring due to human motion in these regions, would be hidden under (or be equal to) the tracking noise-only cycle-slip effects. This minimum C/N_0 threshold is highlighted with a black dotted line in all the figures of this Section, for comparison purposes.

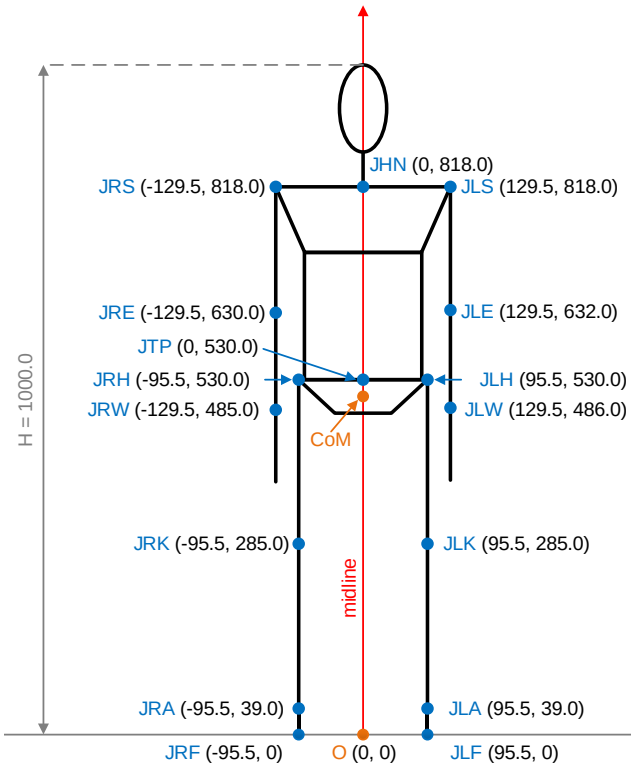

Figure 11. A custom human biomechanical model (HBM)

As shown in Figure 12, tracking noise-only causes no cycle slips for a 29dB-Hz C/N_0 threshold at 20Hz B_{L_CA}, with a gradual C/N_0 threshold decrease to 24dB-Hz at 5Hz B_{L_CA}. The fact that tracking noise-only causes more adverse cycle-slip effects for higher B_{L_CA} values is explained because lower bandwidths smooth the tracking noise input to the PLL. This means that when the simulated third-order PLL operates below 29dB-Hz C/N_0 at 20Hz tracking bandwidth, it will not be able to track carrier phase (range) and almost always lose lock.

Figure 13 illustrates the performance of the simulated PLL, in terms of the minimum C/N_0 required (at various bandwidths) to track motion without experiencing cycle slips, when a user walks 30m in a straight line and the phone is placed at different locations, namely hand, pocket, arm-band and backpack. The plotted lines in Figure 13 show the boundaries between the regions where the simulated PLL succeeds (region highlighted in green) or fails (region highlighted in red) to operate without occurring cycle slips, in the presence of these particular motion profiles or tracking noise only.

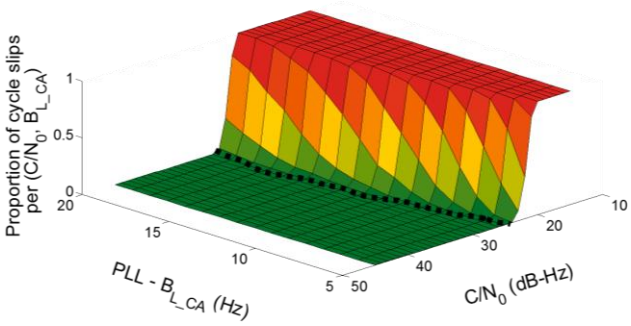

Figure 12. Cycle slips caused to the simulated PLL due to tracking noise (simulated in Matlab)

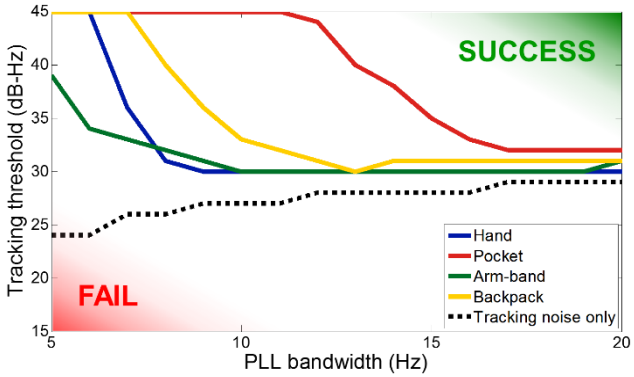

Figure 13. Simulated PLL disruption when a user walks 30m in a straight line, with the phone in various locations

When the phone is in the pocket, the PLL breaks at a higher C/N_0 than the other locations, for all tracking bandwidths, i.e. the performance of the PLL simulator becomes less robust (decreases the "success" region in the plot), compared to the other receiver locations. Having the phone in a backpack, renders the simulated PLL more robust than when it is in the pocket, but less robust than the hand and the arm-band locations.

Holding the phone in the hand, appears to increase the required C/N_0 threshold for tracking motion (without occurring cycle slips) compared to the phone on an arm-band at 5Hz-7Hz bandwidths. At these bandwidths, the arm-band appears to be the most robust location of all, adding a tracking C/N_0 overhead between 7dB-Hz and 15dB-Hz, compared to tracking noise only results. However, at bandwidths above 8Hz, holding the phone in the hand, appears to be slightly more robust than having it on an arm-band. The simulated PLL experienced cycle slips even at good C/N_0 (45dB-Hz), in the presence of motion along any of the NED resolved lines of sight, at bandwidths below 11Hz, 7Hz and 6Hz, when the phone was in a pocket, in a backpack and held by hand, respectively.

The examined phone locations add an overhead (compared to tracking noise only results) between 2dB-Hz (with the phone in the hand) and 7dB-Hz (with the phone in a

pocket) to the C/N_0 threshold required to track motion without occurring cycle slips at 15Hz tracking bandwidth. Similarly, at a 10Hz tracking bandwidth, the tracking C/N_0 overhead, is between 3dB-Hz (phone in hand) and at least 18dB-Hz, when the phone is in the pocket. From Figure 13, it seems that the lower the tracking bandwidth is, the greater the tracking C/N_0 overhead is added due to the various phone locations.

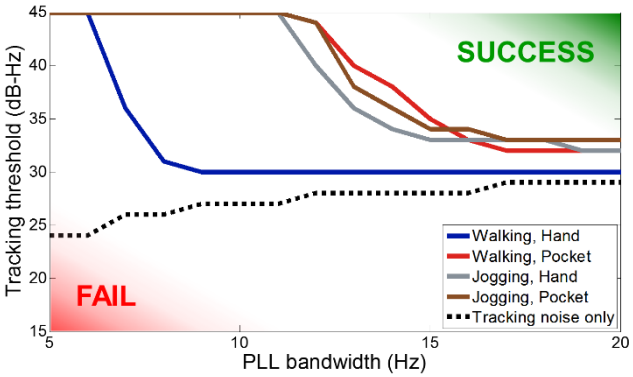

Figure 14. Simulated PLL disruption when a user walks 30m in a straight line, while performing various activities and with the phone in various locations

Figure 14 illustrates the minimum C/N_0 threshold required for the simulated PLL to operate without experiencing cycle slips, in the presence of motion when a user walks or jogs in a straight line for 30m, and the phone is in the pocket or held by hand. As in Figure 13, the plotted lines show the boundaries between the regions where the simulated PLL succeeds and fails to operate without experiencing cycle slips.

The simulated PLL performance is more robust (greater "success" region in the plot) when the user walks holding the phone, than the other input motion profiles, without any cycle slips occurring for a C/N_0 higher than 30dB-Hz, at tracking bandwidths between 9Hz and 20Hz. For all other input motion profiles involving various activities, as illustrated in Figure 14, cycle slips occurred for bandwidths below 11Hz inclusive. Also, at bandwidths higher than 16Hz, having the phone in the pocket while jogging causes the simulated PLL to break at slightly higher C/N_0 values, compared to holding it in the hand or walking having it in the pocket. Generally, jogging seems to render the simulated PLL less robust than walking (reduced "success" region in the plot), although at bandwidths between 13Hz and 15Hz, walking while having the phone in the pocket appears to render the simulated PLL slightly less robust than jogging.

These particular motion profiles, add an overhead between 2dB-Hz and 7dB-Hz to the C/N_0 threshold required to track motion without occurring cycle slips at a 15Hz tracking bandwidth, compared to the tracking noise only C/N_0 threshold. At a 10Hz tracking bandwidth, they add a tracking C/N_0 overhead between 3dB-Hz when the user walks holding the phone and at least 18dB-Hz for the other input motion profiles. Also, the C/N_0 tracking overhead added due to these input motion profiles, appears to increase as the PLL tracking bandwidth decreases.

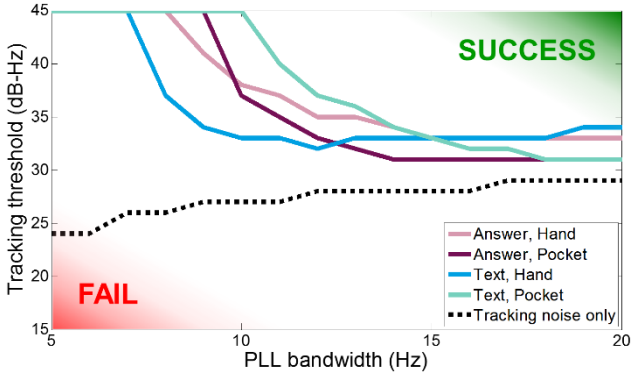

Figure 15. Simulated PLL disruption when a user walks 30m in a straight line, while performing various gestures using the phone and with the phone in various locations

Figure 15 shows the combined effect of various phone locations (hand and pocket) with various gestures (answering and texting) performed by the user. Similar to Figure 13 and Figure 14, the plotted lines show the boundaries between the regions where the simulated PLL succeeds and fails to operate without experiencing cycle slips. Texting while holding the phone appears to disrupt the simulated carrier phase tracking less than the other scenarios at bandwidths up to 13Hz (greater "success" region in the plot). However, at tracking bandwidths above 15Hz, texting while holding the phone causes more adverse disruption to the PLL simulator than the other MoCap scenarios illustrated in Figure 15, by inducing cycle slips at higher C/N_0 values, thus reducing the "success" region in the plot. Also, w.r.t. to a user walking while holding the phone or having the phone on an arm-band (see Figure 13), it is evident that gestures decrease the robustness of the simulated PLL, by adding a higher tracking C/N_0 overhead (reducing the "success" region in the plot).

Also, Figure 15 shows that these particular gestures cannot be tracked by the simulated PLL at bandwidths below 10Hz inclusive. In addition, these gestures add an overhead between 3dB-Hz and 5dB-Hz to the C/N_0 threshold required to track motion without occurring cycle slips at a 15Hz tracking bandwidth, compared to the tracking noise only C/N_0 threshold. At a 10Hz tracking bandwidth, the C/N_0 overhead added due to these gestures is between 6dB-Hz and at least 18dB-Hz, when the user texts after having the phone in the pocket.

5. CONCLUSIONS

This paper proposes and describes a pedestrian motion model (PMM) comprising a human biomechanical model which simulates human movement (including gestures and the GNSS receiver location on the human body), as well as a pedestrian routing model which drives the human biomechanical model between two user-defined locations. The output of the PMM will simulate the 3D trajectory of the GNSS antenna and will be input to the carrier-tracking

simulators in order to recreate the same cycle-slip and false-lock effects as real human motion captured data. The validated PMM will enable Spirent to increase their product offering in the area of simulation-based testing of positioning sensors for pedestrian applications.

The results presented in Section 4, show that typical human motion disrupts the performance of a simulated phase-lock loop (PLL) by inducing cycle slips above the tracking noise-only carrier power-to-noise density ratio (C/N_0) threshold. The C/N_0 tracking overhead added due to human motion (compared to tracking noise-only C/N_0 threshold) appears to increase as PLL tracking bandwidths decrease, since at these bandwidths the simulated PLL cannot track effectively the human motion-induced jerk dynamics.

The location of the phone on the human body seems to cause disruptions in the performance of the simulated PLL, namely having the phone in the pocket renders the simulated PLL less robust than other locations on the human body (hand, arm-band and backpack) at tracking bandwidths between 8Hz and 20Hz. At tracking bandwidths below 8Hz, having the phone on an arm-band caused the simulated PLL to experience the least cycle slips, i.e. the lowest C/N_0 tracking overhead (between 7dB-Hz and 15dB-Hz), compared to tracking noise only results. For bandwidths above 8Hz, holding the phone appears to render the simulated PLL slightly more robust than having it on an arm-band.

Different types of activity (walking or jogging), while holding the phone in the hand or having it inside a pocket, also degrade the simulated PLL performance, since at a 11Hz tracking bandwidth they increase the C/N_0 tracking threshold from 27dB-Hz to 30dB-Hz when a user walks holding the phone in the hand, and up to 45dB-Hz, for the other motion profiles. Generally, jogging seems to render the simulated PLL less robust than walking, although at bandwidths between 13Hz and 15Hz, walking while having the phone in the pocket appears slightly less robust compared to the other motion profiles. Gestures (answering or texting) while the phone is in a pocket or held by hand, disrupts the performance of the simulated PLL more than when a user walks holding the phone, but less than when the user jogs or walks having the phone in a pocket, for bandwidths up to 18Hz.

Consequently, receiver manufacturers should exercise caution before reducing tracking bandwidths to compensate for the reduction in signal to noise levels that can result from smartphone antenna design, human body masking and the effects of buildings, trees and other environmental features. Also, considering that currently smartphones are equipped with inertial sensors of inferior specifications than Xsens MTi-G which was used in this study, it is reasonable to assume that typical human motion involving GNSS equipment has the potential to exceed their output range. This will impact on the navigation solution availability and accuracy, but also needs to be accounted for when implementing inertial sensors' calibration [36][37].

6. FUTURE WORK

Future lines of enquiry of this project will include additional human MoCap scenarios, e.g. boarding a train, ascending/descending staircases or slopes etc., with the motion dynamics resolved along additional lines of sight, in order to represent various GNSS satellites' elevations and azimuths. In addition, the effects of human motion on a simulated frequency-lock loop (FLL) will be investigated and the performance of simulated carrier phase and frequency tracking loops will be validated against other GNSS receivers for accuracy purposes.

The output motion profiles from the custom PMM described in this paper, will be validated against the human MoCap data by Xsens IMU/GPS, to ensure that they cause the same disruptions on the performance of GNSS carrier phase and frequency tracking loops. Finally, it is envisaged to incorporate the context environmental and pedestrian behaviour classes' framework reported in [35], in order to facilitate further study of that research area.

ACKNOWLEDGEMENTS

This work is co-funded by the Engineering and Physical Sciences Research Council (EPSRC) and Spirent Communications plc. The authors would also like to thank Henry Martin, Debbie Walter, Lei Wang and Nikos Papadosifos of UCL, for their help with the human motion capture experiments.

REFERENCES

[1] Groves, P. D., *Principles of GNSS, Inertial and Multisensor Integrated Navigation Systems*, Second Edition, Artech House, 2013.

[2] Misra, P. and Enge, P., *Global Positioning System: Signals, Measurements, and Performance*, Second Edition, Lincoln, MA: Ganga-Jamuna Press, 2006.

[3] Kaplan, E. D. and Hegarty, C., *Understanding GPS: Principles and Applications*, Second Edition, Artech House, 2005.

[4] Racic, V., Pavic, A. and Brownjohn, J. M. W. (2009). "Experimental identification and analytical modelling of human walking forces: Literature review", *Journal of Sound and Vibration*, vol. 326, no. 1–2, pp. 1–49.

[5] Saber-Sheikh, K., Bryant, E. C., Glazzard, C., Hamel, A. and Lee, R. Y. W. (2010). "Feasibility of using inertial sensors to assess human movement", Manual Therapy, vol. 15, no. 1, pp. 122–5.

[6] Xsens, (2010). "MTi-G User Manual and Technical Documentation (Revision H)," Xsens Technologies B.V.

[7] Hamill, J. and Knutzen, K., *Biomechanical basis of human movement*, Third Edition, Wolters Kluwer Health/Lippincott Williams and Wilkins, 2009.

[8] Huston, R. L., *Principles of biomechanics*, vol. 213. Boca Raton, London, New York: CRC Press, 2009.

[9] Human Animation Working Group, "Information technology computer graphics and image processing humanoid animation (H-anim)", *ISO/IEC FCD 19774: 2006*.

[10] Whittle, M. W., *An Introduction to Gait Analysis*, Fourth Edition, Butterworth-Heinemann, 2007.

[11] Novacheck, T., (1998). "The biomechanics of running", *Gait Posture*, vol. 7, no. 1, pp. 77–95.

[12] Orendurff, M. S., Segal, A. D., Klute, G. K., Berge, J. S., Rohr, E. S. and Kadel, N. J. (2004). "The effect of walking speed on center of mass displacement", *J. Rehabilitation Research & Development*, vol. 41, no. 6A, pp. 829-834.

[13] Whittle, M. W., (1997). "Three-dimensional motion of the center of gravity of the body during walking", *Human Movement Science*, vol. 16, pp. 347–355.

[14] Lee, C. R. and Farley, C. T. (1998). "Determinants of the center of mass trajectory in human walking and running", *Journal of Experimental Biology*, vol. 201, no. Pt 21, pp. 2935–44.

[15] Betker, A. L., Moussavi, Z. M. K. and Szturm, T. (2006). "Center of mass approximation and prediction as a function of body acceleration", *IEEE Trans. Biomedical Engineering*, vol. 53, no. 4, pp. 686–93.

[16] Rose, J., Gamble, J. G., Rose, E. and James, G., *Human walking*, Lippincott Williams & Wilkins, 2006.

[17] Thorstensson, A., Nilsson, J., Carlson, H. and Zomlefer, M. R. (1984). "Trunk movements in human locomotion", *Acta Physiologica Scandinavica*, vol. 121, no. 1, pp. 9–22.

[18] Dijkstra, E. W. (1959). "A note on two problems in connexion with graphs," Numerische Mathematik, vol. 1, pp. 269–71.

[19] Dierendonck, A. V., "GPS receivers" in *Global Positioning System: Theory and Applications*, Parkinson, B. W. and Spiker, J. J. J., Eds. Washington, DC: American Institute of Aeronautics and Astronautics, 1996, pp. 329–407.

[20] Ward, P., Betz, J. and Hegarty, C.,"Satellite signal acquisition, tracking, and data demodulation", in *Understanding GPS Principles and Applications*, Second Edition, Washington, DC: Artech House, 2006, pp. 153–241.

[21] Hsu, L.-T., Jan, S.-S., Groves, P. D. and Kubo, N., "Multipath mitigation and NLOS detection using vector tracking in urban environments," *GPS Solutions*, Jun. 2014.

[22] Psiaki, M. and Jung, H. (2002). "Extended Kalman filter methods for tracking weak GPS signals", *Proceedings of the 15th International Technical Meeting of the Satellite Division of The Institute of Navigation (ION GPS 2002)*, pp. 2539 – 2553.

[23] Yang, Y., Zhou, J. and Loffeld, O. (2012). "GPS receiver tracking loop design based on a Kalman filtering approach", *Proceedings ELMAR – 2012*, pp. 121–4.

[24] Kim, K. H., Jee, G. I. and Song, J. H. (2008). "Carrier tracking loop using the adaptive two-stage Kalman filter for high dynamic situations", *International Journal of Control, Automation, and Systems*, vol. 6, pp. 948–953.

[25] Yao, G., Wenqi, W. and Xiaofeng, H. (2011). "High dynamic carrier phase tracking based on adaptive Kalman filtering", *2011 Chinese Control and Decision Conference (CCDC)*, pp. 1245–9.

[26] Gabaglio, V. (2001). "Centralised Kalman filter for augmented GPS pedestrian navigation", *Proceedings of the 14th International Technical Meeting of the Satellite Division of The Institute of Navigation (ION GPS 2001)*, pp. 11–4.

[27] Li, Y., Zhao, M., Zhong, J., Lv, X. and Wang, Y. (2010). "An algorithm based on dynamic compensation for GNSS carrier tracking of weak signal", *2010 12th IEEE International Conference on Communication Technology*, pp. 1184–7.

[28] Razavi, A., Gebre-Egziabher, D. and Akos, D. M. (2008). "Carrier loop architectures for tracking weak GPS signals", *IEEE Transactions on Aerospace and Electronic Systems*, vol. 44, no. 2, pp. 697–710.

[29] Irsigler, M. and Eissfeller, B. (2002). "PLL Tracking Performance in the Presence of Oscillator Phase Noise", *GPS Solutions*, vol. 5, pp. 45–57.

[30] Curran, J. T., Lachapelle, G. and Murphy, C. C. (2012). "Digital GNSS PLL Design Conditioned on Thermal and Oscillator Phase Noise", *IEEE Transactions on Aerospace and Electronic Systems*, vol. 48, pp. 180–96.

[31] Hofmann-Wellenhof, B., Lichtenegger, H. and Wasle, E., *GNSS - Global Navigation Satellite Systems: GPS, GLONASS, Galileo & more*. Springer, 2007.

[32] McAuley, J. H., Rothwell, J. C. and Marsden, C. D. (1997). "Frequency peaks of tremor, muscle vibration and electromyographic activity at 10 Hz, 20 Hz and 40 Hz during human finger muscle contraction may reflect rhythmicities of central neural firing", *Experimental Brain Research*, vol. 114, pp. 525–41.

[33] Allum, J. H., Dietz, V. and Freund, H. J. (1978). "Neuronal mechanisms underlying physiological

tremor", Journal of Neurophysiology, vol. 41, pp. 557–71.

[34] Winter, D., *Biomechanics and motor control of human movement*. New York: John Wiley & Sons, 1990.

[35] Groves, P. D., Martin, H. F. S., Voutsis, K., Walter, D. J. and Wang, L. (2013), "Context Detection, Categorization and Connectivity for Advanced Adaptive Integrated Navigation", *Proc. ION GNSS+ 2013*, pp. 1039–56.

[36] Martin, H. F. S., Groves, P. D., Newman, M. and Faragher, R. (2013). "A new approach to better low-cost MEMS IMU performance using sensor arrays", *Proc. ION GNSS+ 2013*, pp. 2125–42.

[37] Martin, H. F. S., Groves, P. D. and Newman, M., (2013). "The Limits of In-Run Calibration of MEMS and the Effect of New Techniques", *Proc. ION GNSS+ 2014*.